Regularities of decomposition of organic vapors using a photocatalytic air cleaner

I. A. Baturov,[a,b] A. V. Vorontsov,[b] and D. V. Kozlov[b]★

[a]*Novosibirsk State University,*
2 ul. Pirogova, 630090 Novosibirsk, Russian Federation
[b]*G. K. Boreskov Institute of Catalysis, Siberian Branch of the Russian Academy of Sciences,*
5 prosp. Akad. Lavrent´eva, 630090 Novosibirsk, Russian Federation.
Fax: +7 (383 2) 33 1617. E-mail: kdv@catalysis.ru

The kinetics of oxidation of vapors of model air contaminators, *viz.*, acetone, ethanol, and heptane, was studied using a photocatalytic air cleaner. The composition of the oxidation products was determined, and the rates of oxidation of the starting substances were measured. The deep oxidation of the starting substrates to CO_2 and H_2O occurs until their concentration achieves a limiting value. At higher concentrations a "breakthrough" of the starting substrate is observed. Ethanol is oxidized with the formation of intermediate products. The experimental data obtained were approximated by a kinetic model, which includes stages of formation of intermediates and their competitive adsorption. The results of the approximation agree well with the experimental data.

Key words: photocatalysis, air purification, titanium dioxide, mineralization.

Photocatalytic methods for air purification have considerable advantages over other methods. Unlike air purification by adsorption, photocatalytic oxidation leads to complete neutralization of air pollutants forming CO_2 and H_2O as final products, and no regular regeneration of the photocatalyst is usually required. Almost any organic substance even at low concentration can be oxidized under ambient conditions using air oxygen.

Photons with the energy exceeding the TiO_2 band gap ($\lambda < 380$ nm) can induce the transition of electrons from the valence to the conduction band of a photocatalyst resulting in the formation of electron-hole pairs. The latter are initiators of further redox transformations involving adsorbed molecules of organic substances on the photocatalyst surface.[1,2] As a result of a series of these transformations, almost all organic substances could completely be oxidized to CO_2 and H_2O.

The kinetics of photooxidation of organic substances was studied in reactors of different types: batch, flow-circular, fluidized-bed, and coil reactors.[3,4] All reactors described are small devices for laboratory use.

The purpose of the present work is to study the operation of the industrial photocatalytic air cleaner (PAC) designed for use in accomodation space and automobiles. Acetone, ethanol, and heptane were chosen as test substances. These organic compounds are components of solvents and can be found in the air of rooms and automobile cabins.

Experimental

The photocatalytic air cleaner (PAC) (Fig. 1) was placed in a sealed chamber with the volume 6 L. The chamber was included into a flow circuit (Fig. 2). Gas samplers used for chromatographic analysis of the composition of the initial and final reaction mixtures (IRM and FRM, respectively) were placed at the inlet and outlet of the chamber.

The photocatalyst used in the air cleaner was Pt/TiO_2 [5] (0.2% Pt), which was uniformly deposited on a porous poly-

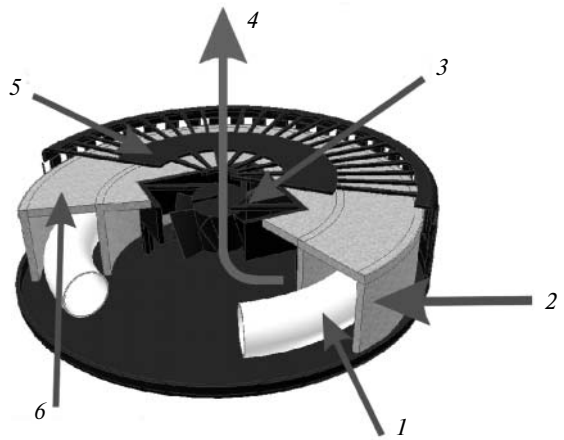

Fig. 1. Aerolaif-BN photocatalytic air cleaner produced at the Luch NPO (Novosibirsk, Russia): *1*, UV lamp; *2*, contaminated air; *3*, ventilator; *4*, purified air; *5*, case; and *6*, filter with photocatalyst.

Published in Russian in *Izvestiya Akademii Nauk. Seriya Khimicheskaya,* No. 8, pp. 1812—1818, August, 2005.

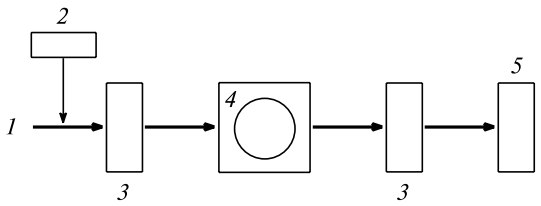

Fig. 2. Scheme of the flow-type system used for experiment: *1*, air flow purified from CO_2, moisture content 50% at 22 °C; *2*, syringe-type pump; *3*, samplers for IRM and FRM; *4*, chamber with PAC; and *5*, foam flowmeter.

meric support (catalyst amount ~3 g). The previous studies showed[6] that dopping TiO_2 with platinum enhances a total rate of the photocatalytic reaction and redistributed intermediate reaction products. When ethanol vapors are photooxidized on the Pt/TiO_2 photocatalyst, carbon monoxide is not formed in the gas phase, although for the use of pure TiO_2 noticeable amounts of CO are observed among the reaction products.[6]

To prepare the IRM, the starting substrate was injected with a syringe-type pump into an air flow with the 50% relative moisture content at room temperature. The device is a platform with a mounted microsyringe. A stop, which pushes the microsyringe plunger, moves slowly along the platform. A volatile component is introduced into the air flow where it evaporates rapidly. Depending on the velocity of syringe pushing, different concentrations of reactants can be created: from zero to those corresponding to the saturated vapor. The concentrations of the reactants in air in a range of 0—10 000 ppm were used. The temperature inside the chamber (320 K) exceeds the ambient temperature by 20 K due to the heat evolved by the working PAC.

The switched-on PAC stirred air inside the chamber with a velocity of 10 $m^3\,h^{-1}$ at flow rates of the IRM and FRM of 0.012 $m^3\,h^{-1}$. The ratio of volume rates of stirring inside the reactor and passing of a mixture through the reactor was 830, which enabled the chamber with the PAC inside to be considered as an ideal stirred reactor. This assumption was used in the mathematical description of the processes under study.

After a new reactant concentration in the IRM was specified, a new stationary state was established within 6—8 h, which approximately tenfold greater than the contact time. The concentrations of the reactants and products in the FRM changed with establishing the stationary state. The concentrations were measured at an interval of 1 h. For analysis of the results, the stationary concentrations of the reactants and products in the FRM were used.

The oxidation rate was calculated by the formula

$$W_{ox} = (C_{IRM} - C_{FRM}) \cdot 10^{-6} \cdot V/(RT)\ (\text{mol min}^{-1}),$$

where C_{IRM} and C_{FRM} are the substrate concentrations in the IRM and FRM, respectively (ppm); V is the gas flow rate (L min^{-1}); $R = 0.082$ L atm mol^{-1} K^{-1} is the universal gas constant; and T is temperature (K).

Gas samples were analyzed on an LKhM-8 chromatograph equipped with a flame-ionization detector and a Paropak-T column ($L = 1$ m, $d = 3$ mm). When studying the CO_2 content, a sample was separated on a carbon column and then passed through a methanation reactor and analyzed using a flame-ionization detector.

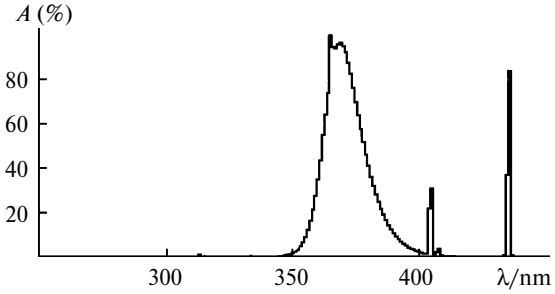

Fig. 3. Emission spectrum of a TL´E 22W/10 lamp (Philips) used in the Aerolaif-BN PAC (data from the manufacturer).

It was assumed in the calculations of the quantum efficiency of photocatalytic processes that the UV radiation of the lamp corresponded to the wavelength 365 nm (Fig. 3) and the fraction of UV radiation was 25% of the electric power of the lamp (22 W), which is typical of the most part of class UV-A commercial low-pressure Hg lamps.

Results and Discussion

Oxidation of acetone. *Experimental data*. On passing through the reactor, the acetone vapors undergo deep oxidation according to the following equation

$$Me_2CO + 4\,O_2 \xrightarrow{h\nu} 3\,CO_2 + 3\,H_2O.$$

The kinetic curves of CO_2 and acetone vapors at the outlet of the chamber *vs.* acetone concentration in the IRM are shown in Fig. 4. No formation of gaseous intermediate products of acetone oxidation was observed in a

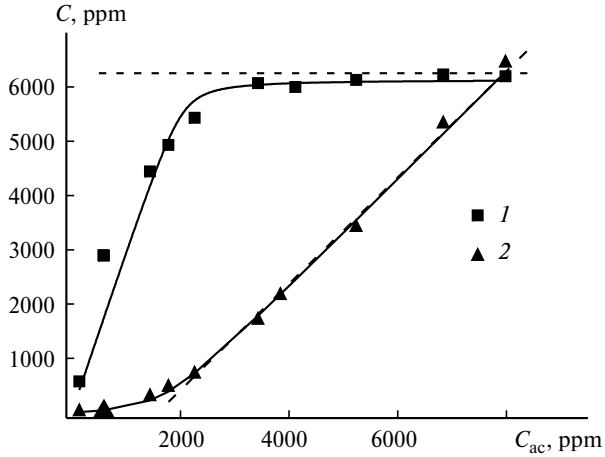

Fig. 4. Change in the concentration of CO_2 and acetone vapors (C) at the outlet of the chamber with the photocatalytic air cleaner at different concentrations of acetone vapors (C_{ac}) in the IRM. Components of the FRM: *1*, CO_2; and *2*, acetone. Solid lines are the approximating curves by the simulation results, and dotted lines are the asymptotic straight lines to which the experimental data approach with an increase in the acetone concentration in the IRM.

wide concentration range, which agrees with our earlier results[5] and data of other authors.[7]

The concentrations of acetone (C_{ac}) and CO_2 in the FRM increase gradually with an increase in the acetone concentration in the IRM from 0 to 2000 ppm. For the further increase in C_{ac} in the IRM, the CO_2 concentration in the FRM remains unchanged, being ~6000 ppm. This implies that the maximum efficiency of the PAC is achieved when C_{ac} in the IRM is 2000 ppm. If C_{ac} in the IRM continues to increase, C_{ac} in the FRM increases by an equivalent value; the rate of complete acetone oxidation remains at the former level. At any acetone concentration in the IRM, the carbon content in the IRM and FRM is the same. This implies that the reactor operates, in fact, under the steady-state conditions and no intermediate oxidation products are accumulated on the photocatalyst surface.

The limiting rate of acetone oxidation, which was achieved in experiment (see Fig. 4), is $1.8 \cdot 10^{-5}$ mol min^{-1}. This allows one to estimate the quantum efficiency of acetone oxidation assuming that 16 photons are needed for the complete oxidation of one acetone molecule.[8] The resulting quantum efficiency is $\varphi = 16 \cdot (W_{ox}/W_q) \cdot 100\% = 34\%$ (W_q is the quantum flux from the lamp, mol min^{-1}).

Simulation of the kinetics of acetone oxidation. To describe the kinetics, we considered the two-step model of acetone oxidation

$$A + Z \underset{}{\overset{K_a}{\rightleftharpoons}} AZ,$$

$$AZ \xrightarrow{k} P + Z,$$

where A is an acetone molecule, Z is an adsorption site, AZ is an acetone molecule adsorbed on the surface, P are the oxidation products (carbon dioxide and water), K_a is the adsorption equilibrium constant of acetone, and k is the rate constant of acetone oxidation. At least two known facts are described in this scheme.

1. At low concentrations the adsorption isotherm of acetone is described by the Langmuir model.[5,9]

2. No gaseous intermediate products are formed in substantial concentrations upon the photocatalytic oxidation of acetone.[5,10,11]

Let us assume that the reaction occurs in an ideal stirred reactor (chamber) with the volume V (L) at the flow rate of the reaction mixture u (L s^{-1}) and content of catalyst active sites N_0 (mol). The concentration of substance A at the inlet is equal to C_A^0 (mol L^{-1}). Since the concentrations are rather low, both flow rates at the inlet and outlet of the reactor are uqual to u. Let θ_A be the fraction of sites on the surface occupied by acetone. The total change in the concentration of reactant A in the chamber involves a change in the concentration of A both in the gas phase dC_A/dt and in the layer adsorbed on the catalyst surface $(N_0/V) \cdot (d\theta_A/dt)$. This change is caused by the introduction and removal of the reactant, as well as its conversion. In other words, the following expression is valid:

$$\frac{dC_A}{dt} + \frac{N_0}{V}\frac{d\theta_A}{dt} = \frac{u}{V}C_A^0 - \frac{u}{V}C_A - \frac{N_0}{V}k\theta_A, \qquad (1)$$

where $\theta_A = (K_aC_A)/(1 + K_aC_A)$.

Under the steady-state conditions, the left part of Eq. (1) is equal to zero, which enables one to derive the following dependence of the concentration of reactant A in the FRM on C_A^0 in the IRM:

$$C_A(C_A^0) = (M + N)/(2K_a), \qquad (2)$$

$$M = K_aC_A^0 - \frac{N_0}{u}kK_a - 1,$$

$$N = \sqrt{(1 - K_aC_A^0 + \frac{N_0}{u}kK_a)^2 + 4K_aC_A^0}.$$

At high C_A^0 the plot $C_A(C_A^0)$ becomes linear

$$C_A(C_A^0) = C_A^0 - N_0k/(2u).$$

This equation is described by a straight line to which the plot of the acetone concentration in the FRM *vs.* its starting concentration in the IRM (see Fig. 4, dotted lines) tends asymptotically. The $N_0k/(2u)$ value corresponds to the maximum acetone oxidation rate in the reactor.

Using Eq. (2), we performed the numerical approximation of the experimental data (see Fig. 4, solid lines). The CO_2 concentrations were approximated by the function $C_{CO_2} = 3(C_{ac}^0 - C_{ac})$. The calculated adsorption constant of acetone ($K_a = 0.06 \pm 0.02$ (ppm)$^{-1}$) differs from the value obtained for other TiO_2 samples ($K_a = 0.0026$ (ppm)$^{-1}$) by an order of magnitude.[5] Perhaps, the adsorption constants can substantially change under photoirradiation and steady-state reaction conditions.

The typical number of active sites N_0 on the surface of the TiO_2 photocatalyst is known[11]: $5 \cdot 10^{14}$ cm^{-2}. Knowing this value, one can estimate the apparent rate constant of acetone oxidation assuming that the whole photocatalyst is irradiated: $k = (2.8 \pm 1) \cdot 10^{-7}$ s^{-1}.

Photocatalytic oxidation of heptane vapors. *Experimental results*. The complete photocatalytic oxidation of the heptane vapors corresponds to the following empirical equation:

$$C_7H_{16} + 11\ O_2 \xrightarrow{h\nu} 7\ CO_2 + 8\ H_2O.$$

In our experiments the only oxidation products detected were CO_2 and water. The plots of the concentrations of heptane and CO_2 at the outlet of the chamber *vs.* heptane concentration at the inlet of the chamber are shown in Fig. 5.

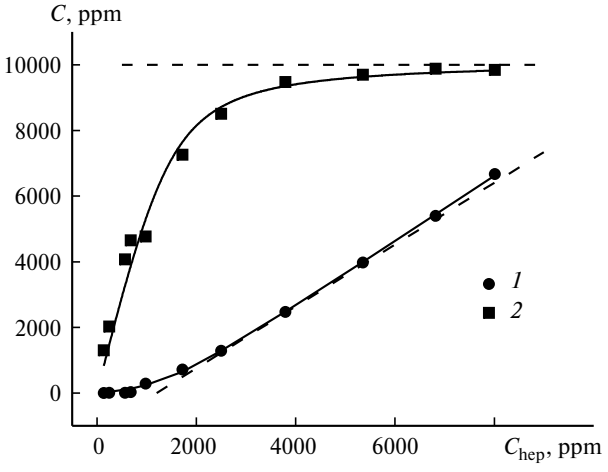

Fig. 5. Change in the concentration of CO_2 and heptane vapors (C) at the outlet of the chamber with the photocatalytic air cleaner at different concentrations of heptane vapors (C_{hep}) in the IRM. Components of the FRM: *1*, heptane; and *2*, CO_2. Solid lines are the approximating curves by the simulation results, and dotted lines are the asymptotic straight lines to which the experimental data approach with an increase in the acetone concentration in the IRM.

The heptane concentration in the FRM increases gradually as the heptane concentration in the IRM increases from ~1000 to 4000 ppm. The CO_2 concentration also increases gradually and reaches a constant level of ~10000 ppm. This means that the maximum productivity of the PAC is achieved at a heptane concentration in the IRM of 4000 ppm and more. The further increase in the heptane content in the IRM results in an increase in the heptane concentration in the FRM by an equivalent value, while the rate of heptane oxidation remains at the former level, which is similar to the situation for acetone oxidation.

As in the case of acetone oxidation, the carbon content in the IRM and FRM is the same for any heptane concentration in the IRM. This indicates that the reactor operates under the steady-state conditions and no intermediate oxidation products are accumulated on the photocatalyst surface.

The limiting rate of deep heptane oxidation achieved in experiments is $1.3 \cdot 10^{-5}$ mol min^{-1}. This makes it possible to estimate the quantum efficiency of the process using assumptions on the photon flux, which are similar to those for acetone. In addition, when estimating the quantum efficiency, we suppose that 44 photons are needed for the complete oxidation of one heptane molecule. This number is equal to the change in the sum of oxidation states of carbon atoms in the empirical equation. The resulting quantum efficiency of photocatalytic heptane oxidation is $\varphi = 44 \cdot (W_{ox}/W_q) \cdot 100\% = 67\%$.

Simulation of heptane oxidation. The two-step model of heptane oxidation, which is completely equivalent to the scheme of acetone oxidation, was used for the simulation of the kinetics of heptane oxidation. In this case, A is a heptane molecule, AZ is a heptane molecule adsorbed on the surface, K_a is the adsorption constant of heptane, and k is the first-order rate constant of heptane oxidation on the photocatalyst surface. It can be assumed that the dependence of the heptane concentration at the outlet of the chamber on the concentration at the inlet of the chamber is also described by Eq. (2).

The numerical approximation of the experimental data on heptane oxidation was performed using Eq. (2) (see Fig. 5, solid lines). The CO_2 concentration was approximated by the function $C_{CO2} = 7(C_{hep}^0 - C_{hep})$, where C_{hep} is the heptane concentration. The calculated values of the adsorption constant of heptane is $K_a = (4.1 \pm 1.5) \cdot 10^{-4}$ (ppm)$^{-1}$. Assuming that the whole catalyst is irradiated, the apparent rate constant (k) of photocatalytic heptane oxidation is $(1.1 \pm 0.37) \cdot 10^{-6}$ s^{-1}.

Photocatalytic oxidation of ethanol vapors. *Experimental data*. Unlike acetone and heptane, ethanol vapors produces intermediate oxidation products of the photocatalytic oxidation, which were detected in the gas phase of the reactor: acetaldehyde, acetic acid, and ethyl acetate, as well as the deep oxidation products (CO_2 and H_2O). Based on these results, the scheme of ethanol oxidation was proposed (Scheme 1). Each step designated by arrow can consist of several successive elementary steps.

Scheme 1

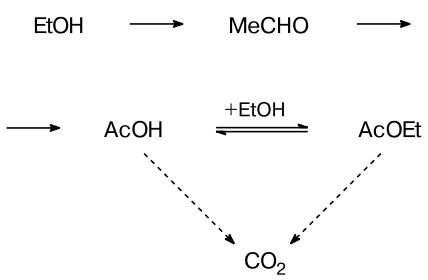

Similar intermediates of the photocatalytic oxidation of ethanol were described previously.[12—14]

We identified ethyl acetate as an intermediate oxidation product only under the steady-state reaction conditions. No formation of ethyl acetate was observed for the photocatalytic oxidation of ethanol under the static conditions. Probably, under the steady-state conditions, the acetic acid that formed interacts with excess ethanol to form ethyl acetate, which is displaced from the photocatalyst surface by other adsorbed compounds.

The plots of the stationary concentrations of ethanol, acetaldehyde, acetic acid, ethyl acetate, and carbon dioxide in the FRM of the chamber *vs.* ethanol concentration in the IRM are shown in Fig. 6. It can be seen that only CO_2 is present in the FRM when the concentration of ethanol in the IRM does not exceed 1000 ppm. In the

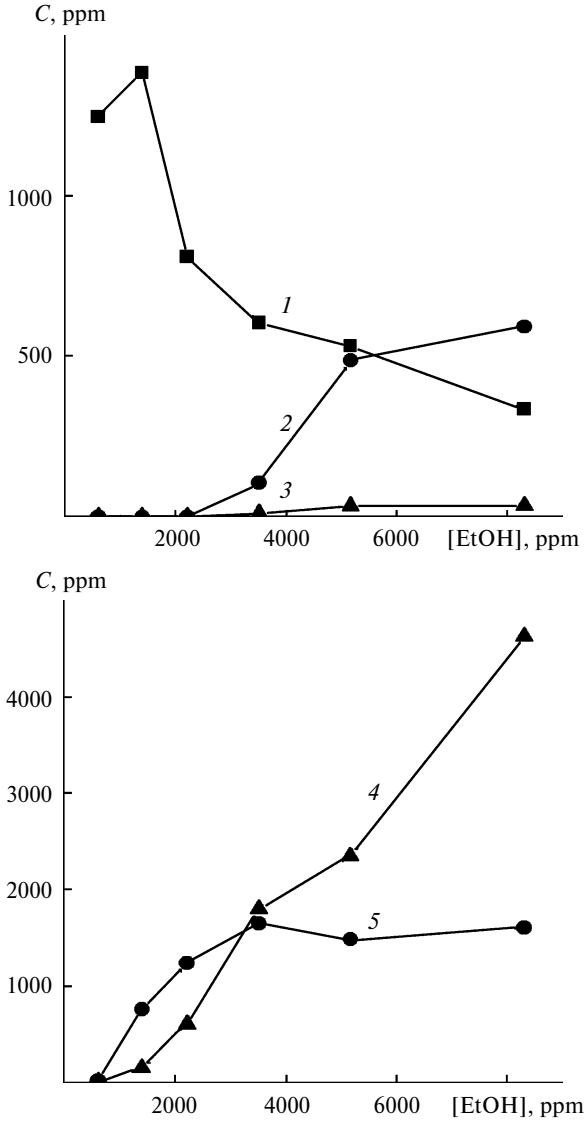

Fig. 6. Concentrations of CO_2 (*1*), AcOH (*2*), AcOEt (*3*), EtOH (*4*), and MeCHO (*5*) at the outlet of the ideal stirred photocatalytic reactor (*C*) *vs.* concentration of ethanol in the IRM.

case of full ethanol oxidation, the theoretical concentration of CO_2 almost coincided with the measured value, which indicates the complete conversion of ethanol to CO_2 and H_2O without accumulation of intermediate products.

With the further increase in the ethanol concentration at the inlet of the reactor, ethanol, acetic acid, acetaldehyde, and ethyl acetate were observed at the outlet of the reactor, and the CO_2 concentration decreased. This implies the competitive adsorption of ethanol and products of its oxidation. The latter are displaced from the surface without further oxidation and, thus, the rate of ethanol conversion to the deep oxidation products (CO_2) decreases.

Simulation of the kinetics of ethanol oxidation in an ideal stirred reactor. To reveal all regularities of the reaction, we studied the two-step model of photooxidation of the ethanol vapors with competitive adsorption of the intermediate products and reactants in an ideal stirred reactor (Scheme 2).

Scheme 2

$$A + Z \underset{}{\overset{K_A}{\rightleftharpoons}} AZ$$

$$AZ \xrightarrow{k_1} BZ$$

$$BZ \underset{}{\overset{K_B}{\rightleftharpoons}} B + Z$$

$$BZ \xrightarrow{k_2} P + Z$$

A is the oxidized substrate; B and P are the intermediate and final oxidation products, respectively;
K_A and K_B are the adsorption constants of substances A and B, respectively, on the photocatalyst surface (L mol^{-1});
k_1 and k_2 are the heterogeneous rate constants of the second and fourth steps, respectively (s^{-1}).

The model is based on an assumption that adsorption sites on the photocatalyst surface are simultaneously the reaction centers.

The proposed scheme does not describe the mechanism of ethanol photooxidation in detail, because it does not reflect all intermediates observed. Since the acetaldehyde concentration exceeds considerably the concentrations of two other intermediates, this kinetic scheme qualitatively corresponds to the main regularities of the ethanol photooxidation.

Let the reaction to occur in an ideal stirred reactor with the volume V (L) at the flow rate of the mixture u (L s^{-1}) involving N_0 moles of active sites of the catalyst and the concentration of substance A at the inlet is C_A^0 (mol L^{-1}). Let us accept that the initial reaction mixture is strongly dilute (in our case, with air) and, hence, the flow rates of the mixture at the outlet and inlet of the reactor are equal to u.

At any moment, the concentrations of all participants of the reaction obey the following system of equations:

$$\frac{dC_A}{dt} + \frac{N_0}{V}\frac{d\theta_A}{dt} = \frac{u}{V}C_A^0 - \frac{u}{V}C_A - \frac{N_0}{V}k\theta_A, \qquad (3)$$

$$\frac{dC_B}{dt} + \frac{N_0}{V}\frac{d\theta_B}{dt} = \frac{N_0}{V}k_1\theta_A - \frac{N_0}{V}k_2\theta_B - \frac{u}{V}C_B, \qquad (4)$$

$$\theta_A = (K_A C_A)/(1 + K_A C_A + K_B C_B), \qquad (5)$$

$$\theta_B = (K_B C_B)/(1 + K_A C_A + K_B C_B), \qquad (6)$$

where θ_A and θ_B are the fractions of sites on the photocatalyst surface occupied by molecules A and B, respectively.

The left parts of Eqs (3) and (4) correspond to the overall change in the amount of oxidized substrate A and intermediate B in the reactor caused by chemical transformations on the surface and introduction and removal of the substance from the reactor by the flow. Equations (5) and (6) describe competitive adsorption of the starting substrate A and intermediate B. When the reaction proceeds under the steady-state conditions, the left parts of Eqs (3) and (4) are equal to zero. Substituting Eqs (5) and (6) into Eqs (3) and (4), we have the following system of nonlinear equations:

$$uC_A^0 = N_0 k_1 \frac{K_A C_A}{1 + K_A C_A + K_B C_B} + uC_A, \qquad (7)$$

$$N_0 k_1 \frac{K_A C_A}{1 + K_A C_A + K_B C_B} = N_0 k_2 \frac{K_B C_B}{1 + K_A C_A + K_B C_B} + uC_B. \qquad (8)$$

Let us introduce designations $k_1' = N_0 k_1/u$ and $k_2' = N_0 k_2/u$ and rewrite the equations in the final form

$$C_A^0 = k_1' \frac{K_A C_A}{1 + K_A C_A + K_B C_B} + C_A, \qquad (9)$$

$$k_1' \frac{K_A C_A}{1 + K_A C_A + K_B C_B} = k_2' \frac{K_B C_B}{1 + K_A C_A + K_B C_B} + C_B. \qquad (10)$$

In essence, Eqs (9) and (10) are the material balance of the system with respect to the starting substrate A and intermediate B.

It seems difficult to solve the system of Eqs (9) and (10) in the general form. Therefore, we restrict our consideration by a particular case when B is adsorbed more weakly than A ($K_A C_A \gg K_B C_B$). In this case, the term $K_B C_B$ in the denominators of Eqs (9) and (10) can be neglected. Then two ultimate cases follow from Eq. (9) $C_A \xrightarrow[C_A^0 \to 0]{} 0$ and $C_A \xrightarrow[C_A^0 \to \infty]{} C_A{}^0 - k_1'$. In practice, this means that at low concentrations $C_A{}^0$ substance A is completely transformed into B and P. At very high concentrations when the whole surface is occupied by molecules A, the rate of decomposition of substance A becomes constant.

The general expression is obtained by the solution of the quadratic equation (9) with respect to the concentration C_A

$$C_A = \frac{1}{2}(C_A^0 - k_1' - 1/K_A) + \frac{1}{2K_A}\sqrt{(1 + k_1' K_A - C_A^0 K_A)^2 + 4K_A C_A^0}. \qquad (11)$$

The concentration of substance B can be expressed through the concentration of substance A as follows:

$$C_B = \frac{C_A^0 - C_A}{k_2' K_B/(1 + K_A C_A) + 1}. \qquad (12)$$

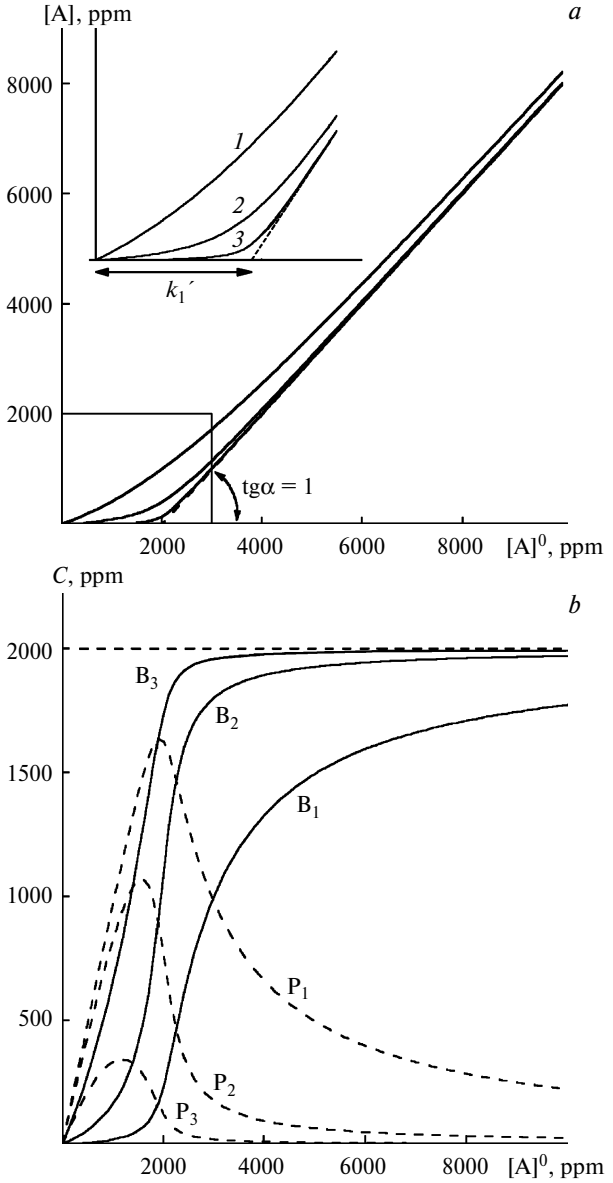

Fig. 7. *a*. Concentration of component A at the outlet of the reactor at different initial concentrations $C_A{}^0$ calculated by Eq. (11). Three different curves were plotted at the same conversion rate constant $k_1' = 2000$ (ppm)$^{-1}$ but different adsorption constants (K_A) of the oxidized substrate. The region marked by rectangle in the main plot is shown in more detail in insert: $K_A = 0.001$ (*1*), 0.01 (*2*), and 0.1 (ppm)$^{-1}$ (*3*). *b*. Concentrations of intermediate B and product P (*C*) at the outlet of the reactor at different initial concentrations of the substrate $C_A{}^0$ calculated by Eq. (12). When plotting the curves, we used the constant values $k_1' = 2000$ (ppm)$^{-1}$ and $K_A = 0.1$ (ppm)$^{-1}$ corresponding to the curve in Fig. 7, *a*; $k_2' \cdot K_B = 100$ (P_1—B_1), 10 (P_2—B_2), and 1 (P_3—B_3).

It can be seen that the product $k_2'K_B$ completely determines a change in the concentration of substance B at the outlet of the reactor. When this value is small, for example, due to a low rate of transformation of B into P, substance B leaves the reactor virtually without further transformation, and its concentration is close to the limiting value $C_B = C_A^0 - C_A = k_1'$. In the case when the value of the product $k_2'K_B$ is high, substance B can be transformed into P almost completely at the initial step. Then the concentration of B at the outlet is close to zero. This model also predicts that the concentration of the final product P passes through a maximum and the conversion tends to zero in the limit, at a high concentration of the starting substance.

All described regularities, which were obtained by Eqs (11) and (12), are plotted in Fig. 7.

The experimentally measured dependence of the CO_2 concentration in the FRM on the ethanol concentration in the IRM (see Fig. 6, *a*) shows that the conversion of alcohol to the final product CO_2 decreases indeed with an increase in the concentration of the starting substrate in the IRM.

The results of the nonlinear approximation of the experimental data by the theoretical curves calculated from Eqs. (11) and (12) for ethanol and acetaldehyde are shown in Fig. 8.

Under an assumption that the whole photocatalyst surface is irradiated in the reactor, the adsorption constants of the reactant (A) and intermediate product (B) are 0.5 and 0.32 $(ppm)^{-1}$, respectively, and the rate constant of photocatalytic oxidation k_1 and k_2 are $5 \cdot 10^{-6}$ and $1.7 \cdot 10^{-7}$ s^{-1}, respectively.

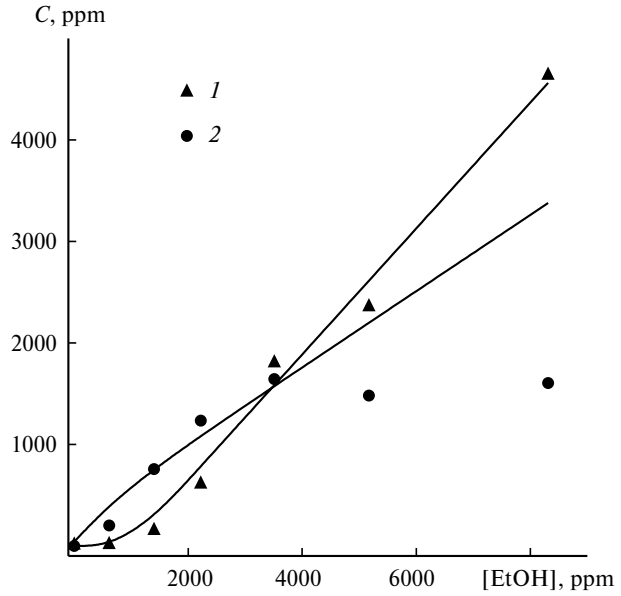

Fig. 8. Concentrations of ethanol (*1*) and acetaldehyde (*2*) at the outlet of the ideal stirred photocatalytic reactor (*C*) *vs.* concentration of ethanol in the initial reaction mixture approximated by the theoretical curve.

The proposed kinetic scheme qualitatively describes the experimentally observed change in the concentration of the ethanol vapors. In addition, the obtained adsorption rate constants for ethanol agree well with published data.[12]

* * *

Thus, the following conclusions can be drawn.

1. Reactions of photocatalytic oxidation of acetone and heptane vapors in a flow-type photocatalytic ideal stirred reactor proceed completely to form CO_2 and H_2O without formation and desorption of intermediate oxidation products to the gas phase. The quantum efficiencies of acetone and heptane oxidation in the reactor are approximately 34 and 67%, respectively.

2. The two-step kinetic model of photocatalytic oxidation of acetone and heptane, including the step of reversible substrate adsorption and irreversible photocatalytic oxidation to the final products, well describes the experimental data. The values of adsorption constants obtained by the nonlinear approximation of the experimental data are close to published values.

3. Intermediate oxidation products, *viz.*, acetaldehyde, acetic acid, and ethyl acetate, were found to evolve to the gas phase during the photocatalytic oxidation of the ethanol vapors. For a small ethanol concentration (<1000 ppm) at the inlet of the reactor, no evolution of intermediates is observed.

4. The four-step kinetic scheme for the photocatalytic oxidation of the ethanol vapors, including the steps of formation of the intermediate and final reaction products and the reversible competitive adsorption of the substrate and intermediate, was proposed. The results obtained using this model agree qualitatively with the experimental data.

5. It is shown that at high concentrations of ethanol (>1000 ppm) the products of incomplete oxidation are displaced from the TiO_2 surface due to competitive adsorption.

This work was financially supported by the Russian Science Support Foundation, the Finnish Academy of Sciences (Program "Russia in Flux," Grant 208134), and the CRDF (Grant NO-008-X1).

References

1. M. A. Fox and M. T. Dulay, *Chem. Rev.*, 1993, **93**, 341.
2. M. R. Hoffman, S. T. Martin, W. Choi, and D. W. Bahnemann, *Chem. Rev.*, 1995, **95**, 96.

3. *Photocatalytic Purification and Treatment of Water and Air*, Eds D. F. Ollis and H. Al-Ekabi, Elsevier, Amsterdam, 1993, p. 481.
4. A. V. Vorontsov, D. V. Kozlov, P. G. Smirniotis, and V. N. Parmon, *Kinet. Katal.*, 2005, **46**, 466 [*Kinet. Catal.*, 2005, No. 3 (Engl. Transl.)].
5. A. V. Vorontsov, I. V. Stoyanova, D. V. Kozlov, V. I. Simagina, and E. N. Savinov, *J. Catal.*, 2000, **189**, 360.
6. A. V. Vorontsov and V. P. Dubovitskaia, *J. Catal.*, 2004, **221**, 102.
7. M. L. Sauer and D. F. Ollis, *J. Catal.*, 1994, **149**, 81.
8. D. V. Kozlov, A. A. Panchenko, D. V. Bavykin, E. N. Savinov, and P. G. Smirniotis, *Izv. Akad. Nauk*, *Ser. Khim.*, 2003, 1041 [*Russ. Chem. Bull., Int. Ed.*, 2003, **52**, 1100].
9. J. M. Coronado, M. E. Zorn, I. Tejedor-Tejedor, and M. A. Anderson, *Appl. Catal. B: Env.*, 2003, **43**, 333.
10. A. V. Vorontsov, G. B. Barannik, O. I. Snegurenko, E. N. Savinov, and V. N. Parmon, *Kinet. Katal.*, 1997, **38**, 97 [*Kinet. Catal.*, 1997, **38** (Engl. Transl.)].
11. M. L. Sauer and D. F. Ollis, *J. Catal.*, 1996, **163**, 215.
12. M. R. Nimlos, E. J. Wolfrum, M. L. Brewer, J. A. Fennell, and G. Bintner, *Environ. Sci. Technol.*, 1996, **30**, 3102.
13. M. L. Sauer and D. F. Ollis, *J. Catal.*, 1996, **158**, 570.
14. D. S. Muggli, J. T. McCue, and J. L. Falconer, *J. Catal.*, 1998, **173**, 470.

Received April 27, 2004